

Article

Experimental and Simulation-Based Study on Thermal Runaway Characteristics of 18650 Lithium-Ion Batteries and Thermal Propagation Patterns in Battery Packs

Yao Yao ¹, Xu Peng ², Lei Gao ³, Haozhe Xing ¹, Xiaohui Xu ¹, Juan Gu ¹, Lu Liu ¹, Songlin Yue ¹, Yanyu Qiu ¹, Youning Wang ¹ and Zhi Zhang ^{3,*}

- ¹ State Key Laboratory for Disaster Prevention & Mitigation of Explosion & Impact, Army Engineering University of PLA, Nanjing 210007, China; yslseu@hotmail.com (S.Y.)
² School of Chemistry and Chemical Engineering, Nanjing University of Science and Technology, Nanjing 210007, China
³ Position Engineering Research Office, Army Engineering University of PLA, Nanjing 210007, China
* Correspondence: zhangnjjn@outlook.com

Abstract: The thermal runaway of lithium-ion batteries is a critical factor influencing their safety. Investigating the thermal runaway characteristics is essential for battery safety design. In this study, the thermal runaway characteristics of 18650 lithium-ion batteries under different SOCs were systematically analyzed by experiment and simulation. It was found that at high SOC (100%), the highly lithium state accelerated lattice oxygen release, promoted the formation of LiNiO and intensified electrolytic liquid oxygenation combustion, while at low SOC (20%), the reduction environment dominated, and the metal Ni and residual graphite were significantly enriched. Gas analysis shows that CO₂ and H₂ account for more than 80%, and their proportion is regulated by SOC. Temperature and pressure monitoring showed that the increase in SOC significantly increased the thermal runaway peak temperature (100% SOC up to 508.4 °C) and pressure (0.531 MPa). The simulation results show that when the battery pack is out of control, the ejection fire and explosion pressure wave are concentrated in the middle and upper region (overpressure up to 0.8 MPa). This study reveals the mechanism by which SOC affects the path of product and gas generation by regulating the oxidation/reduction balance, which lays a theoretical and simulation foundation for the safe design of batteries and the quantitative evaluation of thermal runaway.



Academic Editor: Michele Vittadello

Received: 23 March 2025

Revised: 6 May 2025

Accepted: 12 May 2025

Published: 21 May 2025

Citation: Yao, Y.; Peng, X.; Gao, L.; Xing, H.; Xu, X.; Gu, J.; Liu, L.; Yue, S.; Qiu, Y.; Wang, Y.; et al. Experimental and Simulation-Based Study on Thermal Runaway Characteristics of 18650 Lithium-Ion Batteries and Thermal Propagation Patterns in Battery Packs. *Batteries* **2025**, *11*, 202. <https://doi.org/10.3390/batteries11050202>

Copyright: © 2025 by the authors. Licensee MDPI, Basel, Switzerland. This article is an open access article distributed under the terms and conditions of the Creative Commons Attribution (CC BY) license (<https://creativecommons.org/licenses/by/4.0/>).

Keywords: lithium-ion battery; thermal runaway; SOC; solid-phase products

1. Introduction

As the global energy structure transitions towards cleaner and low-carbon solutions, lithium-ion batteries have emerged as a core power source in new energy vehicles, energy storage stations, and consumer electronics due to their high energy density and long cycle life [1–6]. Among them, the 18650 cylindrical battery has secured a significant position in early Tesla models, drone power systems, and other applications through standardized manufacturing processes and exceptional cost-effectiveness [7–11]. However, lithium batteries are prone to thermal runaway (TR) under thermal abuse conditions (such as external high temperatures or localized overheating), potentially triggering intense combustion explosions and even module-level chain reactions that could lead to major safety incidents [11–17]. For instance, a 2020 incident involving a brand's electric vehicle

catching fire due to battery pack overheating demonstrated how the energy released by high state-of-charge (SOC) batteries under overheating conditions significantly intensified combustion severity, as revealed by subsequent accident investigations.

It is noteworthy that the state of charge (SOC), as a direct indicator of a battery's energy status, profoundly influences its thermal runaway behavior [18–22]. High-SOC batteries (e.g., SOC = 100%) exhibit greater heat release from decomposition reactions due to the highly lithiated state of cathode active materials (e.g., NCM), along with enhanced electrolyte oxidation activity [16]. Conversely, low-SOC batteries (e.g., SOC = 20%), despite their lower chemical energy reserves, face increased risks of lithium plating on the anode that may accelerate internal short circuits. These characteristics result in significant differences in failure modes and hazard severity among batteries at varying SOC levels under overheating scenarios. However, existing research predominantly focuses on single SOC conditions or simplified thermal abuse models, leaving a critical gap in systematic understanding of SOC-thermal runaway coupling mechanisms, which constrains the development of precise battery safety strategies.

In recent years, global scholars have conducted systematic investigations into lithium-ion battery thermal runaway [14,20,23–28]. At the fundamental level, Wang and Feng et al. summarized the mechanism of fire and explosion caused by thermal runaway of lithium batteries [12,29]; Li et al. demonstrated using synchrotron radiation X-ray imaging and in situ transmission electron microscopy that the violent exothermic reaction is triggered by the released oxygen [30]. Zhang et al. revealed the evolution of the failure mechanism of lithium-ion batteries under different characteristic voltages during dynamic overcharging by means of fragmentation analysis, and used multi-scale thermal testing to clarify the dynamic change of the thermal stability of battery components [31]. Liu et al. found through an in situ technique that chemical crosstalk between cathode and anode is a hidden thermal runaway mechanism at high temperatures, and cathodes with poor thermal stability may trigger TR more strongly [32]. Finegan et al. observed the dynamic process of internal short circuit caused by diaphragm collapse through synchrotron radiation X-ray imaging technology [33]. In the study on the effect of SOC, Zhang et al. found that increasing SOC from 50% to 100% can increase the peak temperature of thermal runaway by about 40%, but the quantitative effect on its trigger threshold (such as T_0) is not clear [34]. Xu et al. found that with the decrease in the state of charge, the internal heat propagation speed and surface temperature of the lithium-ion battery decreased [16]. Zhang et al. found that with the increase in SOC, the lower explosive limit (LEL) and alkane content first increased and then decreased [35]. However, current research still faces key challenges: First, dynamic tracking of how SOC regulates the co-evolution pathways of temperature–pressure–gas release remains insufficient. Second, most thermal runaway experiments rely on simplified single-cell models, neglecting the multi-physics coupling effects (thermal–electrical–mechanical) in battery modules, thereby failing to reflect thermal propagation patterns in practical engineering applications.

This study employs a self-developed thermal runaway experimental platform for 18650 lithium-ion batteries to conduct single-cell experiments. Through multi-scale testing and multi-physics modeling, it quantitatively investigates thermal runaway triggering thresholds (temperature, voltage), gas release characteristics, and flame propagation patterns under different SOC levels, revealing critical combustion–explosion features of 18650 batteries. A temperature–pressure–fluid dynamics coupled model is established using the COMSOL Multiphysics Simulation Platform (2024) to elucidate the dynamic evolution from single-cell failure to module-level chain reactions. This work provides essential theoretical support for designing and developing high-safety lithium-ion battery systems, contributing to the continuous improvement of lithium battery pack stability.

2. Materials and Methods

The battery is a commercial 18650 lithium-ion battery (nominal capacity 3.5 Ah, voltage 3.6 V). The cathode material of the battery is $\text{LiNi}_{0.6}\text{Co}_{0.2}\text{Mn}_{0.2}\text{O}_2$ (NCM622), the anode material is graphite, the electrolyte is 1 M LiPF_6 , and the diaphragm is a PE-based ceramic coating. According to the different SOC levels of the battery, the battery is further divided into five experimental groups. The constant current discharge method (0.1 C discharge to 2.5 V) was used to calibrate the actual capacity, and electrochemical impedance spectroscopy (EIS) was used to detect the battery health (SOH > 95%).

First, let the battery stand in a 25 °C incubator for 24 h to ensure that the temperature and SOC are evenly distributed. Thermocouples (positive pole, negative pole, side wall center) are arranged on the surface of the battery. Then, put the battery in the thermal runaway test chamber of the lithium-ion battery, wrap the side of the battery with a ceramic heater (power density 0.5 w/cm²) (coverage ≥ 90%), start the heating process, and the heating rate is 5 °C/min. When detecting the self-exothermic (T_0) reaction of a lithium-ion battery, stop the external power heating and switch to the adiabatic mode, and continue monitoring until the end of thermal runaway. During the experiment, the temperature–pressure–time curve was recorded synchronously, and the gas generated after the thermal runaway of the lithium-ion battery was collected and analyzed, and the battery debris was recovered for phase analysis to determine the reaction products.

The experimental platform uses the 18650 lithium-ion battery thermal runaway experimental platform built by the research group, which is composed of an adiabatic test chamber, battery thermal runaway triggering equipment, and battery thermal runaway process parameter testing equipment. The thermodynamic data were collected via a Thermal Hazard Technology (ARC) infrared thermal imager with a resolution of 640 × 480 and accuracy of ±1 °C (FLIR A655sc, FLIR Systems, Wilsonville, OR, USA) and K-type thermocouple array. The electrochemical parameters of the battery were collected by a battery tester (Neware BTS-4000, Neware Technology Limited, Dongguan, China) with a voltage accuracy of ±0.1 mV and an electrochemical workstation (Gamry 3000, Gamry Instruments, Philadelphia, PA, USA). The experimental gas production characteristics were analyzed by Agilent 7890b-5977a (Agilent Technologies, Palo Alto, CA, USA) gas chromatography–mass spectrometry (GC–MS). The flame characteristics in the process of thermal runaway were collected by a 1280 × 800 high-speed camera (Phantom V2512, 10,000 fps, Vision Research, Wayne, NJ, USA). The thermal runaway solid phase products of Li-ion batteries were analyzed by XRD (Bruker D8 Advance, Bruker, Karlsruhe, Baden-Württemberg, Germany), IR (Nicolet, Magna IR 560, Thermo Fisher Scientific, Waltham, MA, USA), and RAMAN (LabRAM HR Evolution, HORIBA Scientific, Saint-Etienne, France).

This experiment was completed in the 18650 lithium-ion battery thermal runaway experimental platform, which was built of high-strength steel and equipped with a high-speed pressure relief valve (response time < 10 ms). The experiment adopts a remote trigger and automatic data collection to avoid personnel exposure risk. Regarding the control of experimental uncertainty, the SOC error of the lithium-ion battery is calibrated by means of the mean value method (e.g., via three cycles of charge and discharge). The repeatability was verified by repeating the experiment three times for each group of SOC conditions to eliminate abnormal values.

3. Results and Discussion

3.1. Characterization of Thermal Runaway Products

3.1.1. Characterization of Thermal Runaway Solid Phase Products

The XRD pattern of solid phase products produced by the thermal runaway reaction of the 18650 lithium-ion battery under overheating conditions is shown in Figure 1a.

The XRD patterns of the products after thermal runaway of lithium-ion batteries under different SOC conditions (20%, 60%, and 100%) showed that the peak positions of the XRD patterns of the products after thermal runaway of lithium-ion batteries under the three SOC conditions were basically the same. The main diffraction peaks are $2\theta = 26.58^\circ, 37.28^\circ, 38.46^\circ, 43.32^\circ, 44.48^\circ, 51.84^\circ, 62.82^\circ$. The sharp peak of 26.58° in the spectrum corresponds to the (003) crystal face of graphite (PDF#26-1079), indicating that the negative graphite is not completely oxidized at high temperature and there is residual crystalline carbon. The sharp peaks of 38.46° and 44.48° correspond to (012) and (104) crystal planes of LiNiO, respectively, which are derived from the high temperature decomposition of NCM cathode ($\text{LiNi}_{0.6}\text{Co}_{0.2}\text{Mn}_{0.2}\text{O}_2 \rightarrow \text{LiNiO} + \text{CoO} + \text{MnO} + \text{O}_2\uparrow$). The strength increases with the increase in SOC, because the positive lithium-rich state accelerates the release of lattice oxygen and promotes the transition of layered structure to anoxic LiNiO phase at high SOC [29]. The half width peaks of 37.28° (LiCoO_2 , (222)) and 62.82° (LiCoO_2 , (440)) are related to the partial reduction of Co^{3+} to Co^{2+} ($\text{LiCoO}_2 \rightarrow \text{LiCoO} + \frac{1}{2}\text{O}_2\uparrow$) and the peak position shift ($\pm 0.2^\circ$) is due to the lattice distortion caused by the formation of solid solution by Mn/Ni doping. The sharp peaks of 44.48° ($\text{Ni}, (111)$) and 51.84° ($\text{Ni}, (200)$) indicate that the metal elemental formation of $\text{Ni}^{3+} \rightarrow \text{Ni}^0$ ($\text{LiNiO} \rightarrow \text{Ni} + \text{Li}_2\text{O} + \frac{1}{2}\text{O}_2\uparrow$) in the deep reduction environment has higher strength at low SOC (20%), because the lithium-positive electrode is more prone to reduction reaction [12]. The consistency of peak positions under the three kinds of SOCs reflects that the main reaction path of thermal runaway is similar, but the difference in peak intensities reveals that SOC affects the product ratio by regulating the oxidation/reduction balance: under high SOC (100%), O_2 release intensifies the combustion of electrolyte and generates CO/CO_2 , which inhibits the formation of metal Ni; low SOC (20%) led to the reduction environment, which promoted the enrichment of Ni and residual graphite. XRD analysis showed that the thermal runaway product was a heterogeneous mixture of LiNiO, LiCoO, Ni and residual graphite, and its microstructure defects (such as oxygen vacancy and solid solution doping) were the main reasons for the broadening and deviation of peak shape, which provided a key phase basis for quantifying the degree of thermal runaway reaction and optimizing the safety design of battery.

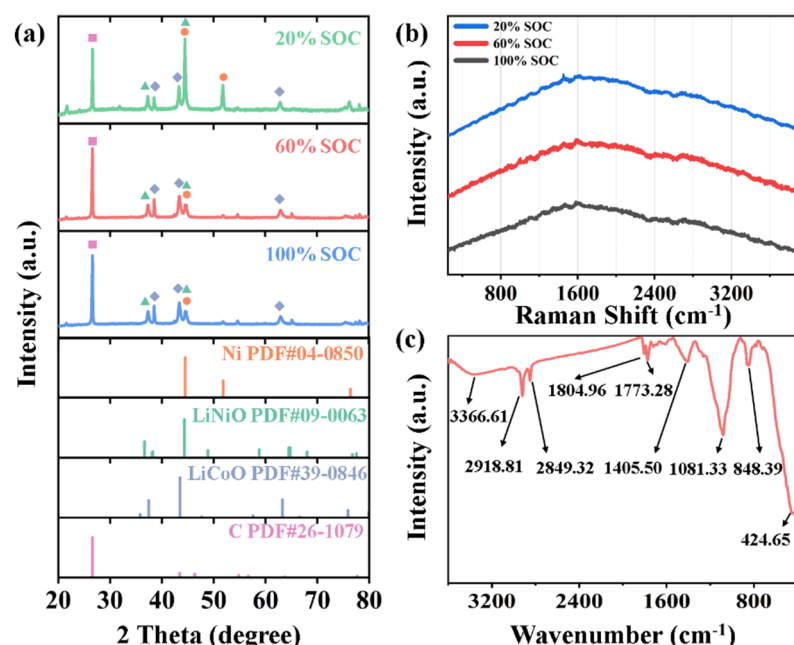


Figure 1. XRD patterns (a), Raman spectra (b), and infrared spectra (c) of solid-phase products from lithium-ion battery thermal runaway.

Figure 1b shows the Raman spectra of the products after thermal runaway of lithium-ion batteries under different SOC conditions (20%, 60%, and 100%). Since the reaction products of thermal runaway of lithium-ion batteries are heterogeneous mixed systems, no obvious D peak or G peak is found in the Raman spectra. However, by comparing the Raman spectra of the products after thermal runaway of lithium-ion batteries under three SOC conditions (20%, 60%, and 100%), it can be found that the change trend of the Raman spectra curve is basically the same in the range of 400–3600 cm^{−1}, indicating that the solid-phase products (including LiNiO, LiCoO, Ni, etc.) under thermal runaway of lithium-ion batteries are less affected by the SOC state of the batteries. This conclusion is consistent with the relevant conclusions in XRD analysis.

Figure 1c shows the infrared spectrum of solid-phase products after thermal runaway of a lithium-ion battery under 100% SOC conditions. Combined with the analysis of thermal runaway reaction mechanism of lithium-ion battery, it can be found that the strong absorption peaks at 2918.81 cm^{−1} and 2849.32 cm^{−1} in the figure belong to the symmetric and antisymmetric stretching vibration of C–H bond, mainly from alkane residues (such as –CH₃ and –CH₂) generated by the high-temperature cracking of electrolyte solvent, which is due to the decarboxylation reaction of solvent molecules (such as EC) at high temperature (EC → CO₂↑ + C₂H₄↑ + C_nH_{2n+2}) [36], leading to the deposition of long-chain hydrocarbons on the electrode surface. The strong absorption peaks at 1804.96 cm^{−1} and 1773.28 cm^{−1} are attributed to the stretching vibration of ester group (C=O) and anhydride (C=O), which is due to the reaction between oxygen (O₂) released from the positive electrode and the electrolyte (EC + O₂ → –COOH + CO₂↑) [37]. Under high SOC, the lithium-rich positive electrode intensifies the release of oxygen and promotes the oxidation of esters. The strong absorption peaks at 1405.50 cm^{−1} and 1081.33 cm^{−1} belong to the antisymmetric stretching vibration of CO₃^{2−} and the stretching vibration of the C–O–C ether bond. The strong absorption peaks at 848.39 cm^{−1} and 424.65 cm^{−1} are caused by the bending vibration of PF₆ and the lattice vibration of metal oxides (such as LiCoO₂), respectively. In addition, there is a weak absorption peak at 3366.61 cm^{−1}, which is caused by the O–H stretching vibration and can be attributed to the hydroxyl (–OH) or carboxylic acid group (–COOH) adsorbed on the carbon material surface. The infrared spectra of the solid-phase products after thermal runaway of lithium-ion battery under 100% SOC showed that the electrolyte dominated the reaction, and the ester oxidation and condensation formed a polymer network, which aggravated the thermal runaway exothermic reaction of lithium-ion battery. At the same time, the reaction leads to the collapse of the positive structure, and the layered NCM is transformed into anoxic metal oxides (LiNiO, LiCoO), accompanied by lattice distortion.

3.1.2. Characterization of Thermal Runaway Gas Phase Products

The composition of gas generated after thermal runaway of the lithium-ion battery is shown in Table S1. It can be found that lithium-ion battery overheating out of control will produce a large number of organic and flammable gases, including methane (CH₄), carbon monoxide (CO), carbon dioxide (CO₂), hydrogen (H₂), ethylene (C₂H₄), and other olefin gases (OO). The CO₂ may come from the thermal decomposition of SEI film, the thermal decomposition of lithium carbonate, the thermal decomposition of electrolyte lithium salt LiPF₆, and the combustion of electrolyte. Hydrocarbon gas may come from the reaction between the electrolyte solvent and lithium. The main sources of CO are the reaction of Li embedded in the negative electrode with CO₂ and the reaction of Li embedded in the negative electrode with electrolyte. H₂ may come from the reaction of electrode binders, polyvinylidene fluoride (PVDF), and sodium carboxymethyl cellulose (CMC) with Li [38].

For a lithium-ion battery under any SOC state, CO_2 and H_2 are the two gases with the largest proportion, accounting for more than 80%.

Further, the correlation between the composition proportion of gas produced by thermal runaway and the content of gas components is analyzed, and the results are shown in Figure 2. In Figure 2, PC1 mainly characterizes the oxidation-reduction reaction equilibrium. The high negative load of CO_2 reflected a significant negative correlation with $\text{H}_2/\text{C}_2\text{H}_4$. This indicated that O_2 release at high SOC promoted electrolytic liquid oxygen to CO_2 and inhibited the formation of the reducing gas ($\text{H}_2/\text{C}_2\text{H}_4$). This is also consistent with the relevant conclusions in XRD analysis. According to the principal component analysis diagram (Figure 2a), under the condition of high SOC (100%), the composition of gas production is dominated by CO_2 and concentrated in the negative direction of PC1, which matches the strong oxidation environment. When the SOC is low (20%), the composition of gas production is dominated by $\text{H}_2/\text{C}_2\text{H}_4$, which is concentrated in the positive direction of PC1, indicating that the reducing gas is enriched at this time. At medium SOC conditions (40–80%), the gas-producing components are distributed along the PC2 direction, which indicates that CO/CH_4 is in dynamic equilibrium. At the same time, the correlation analysis of gas-producing components showed that the correlation coefficient of CO_2 and H_2 was -0.98 , showing a strong negative correlation, indicating the competitive mechanism of oxidation (CO_2) and reduction (H_2) reactions in the thermal decomposition process of lithium-ion batteries. The correlation coefficient of CH_4 and CO was 0.68, which was positively correlated, which may indicate that they were jointly derived from the incomplete decomposition of electrolyte solvent (EC/DMC). OO has a weak correlation with the variables, indicating that its source is independent of the main reaction process of lithium-ion battery thermal runaway. In general, the thermal runaway gas generation behavior of lithium-ion batteries is regulated by SOC, showing a significant gradient effect. A large amount of CO_2 enrichment is dominated by the oxidation process at high SOC, while the reduction process is dominant at low SOC, and the contents of H_2 and C_2H_4 increase, while the synergistic effect of pyrolysis and oxidation is reflected at medium SOC.

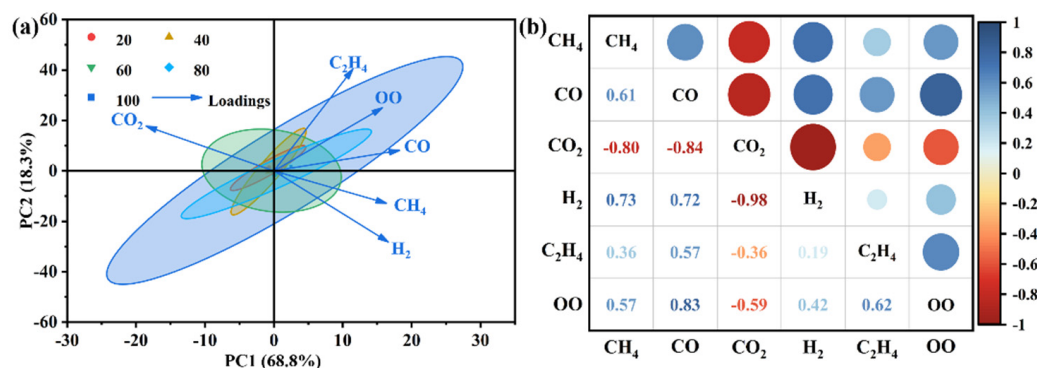


Figure 2. Principal component analysis (PCA) plots (a,b) of gas production from lithium-ion battery thermal runaway.

3.2. Thermal Runaway Processes Under Different SOCs

The variation in temperature and pressure in the positive direction of the lithium-ion battery thermal runaway with reaction time under different SOC conditions is shown in Figure 3. As for the temperature, it can be seen that with the increase in SOC, the peak temperature in the positive direction is also gradually increasing. When the SOC is 100%, the peak temperature reaches 508.4°C . At the same time, combined with the analysis of reaction time, it is found that with the increase in SOC, the time when the lithium-ion battery thermal runaway reaches the peak temperature presents a forward trend. This

phenomenon is due to the fact that the reaction between the positive and negative electrodes in the lithium battery is completed through the migration and recombination of ions. When the battery is in a high charge state, the lithium-ion concentration on the positive electrode is higher, while the lithium-ion concentration on the negative electrode is lower. This unbalanced state will lead to the acceleration of the ion migration rate, thus accelerating the reaction rate between the positive and negative electrodes. At the same time, the resistance distribution in the battery is uneven due to the difference in ion concentration under a high charge state. This will lead to high resistance in some areas inside the battery and large power loss when the current passes through. These high-resistance areas will focus on generating more heat, resulting in an increase in temperature.

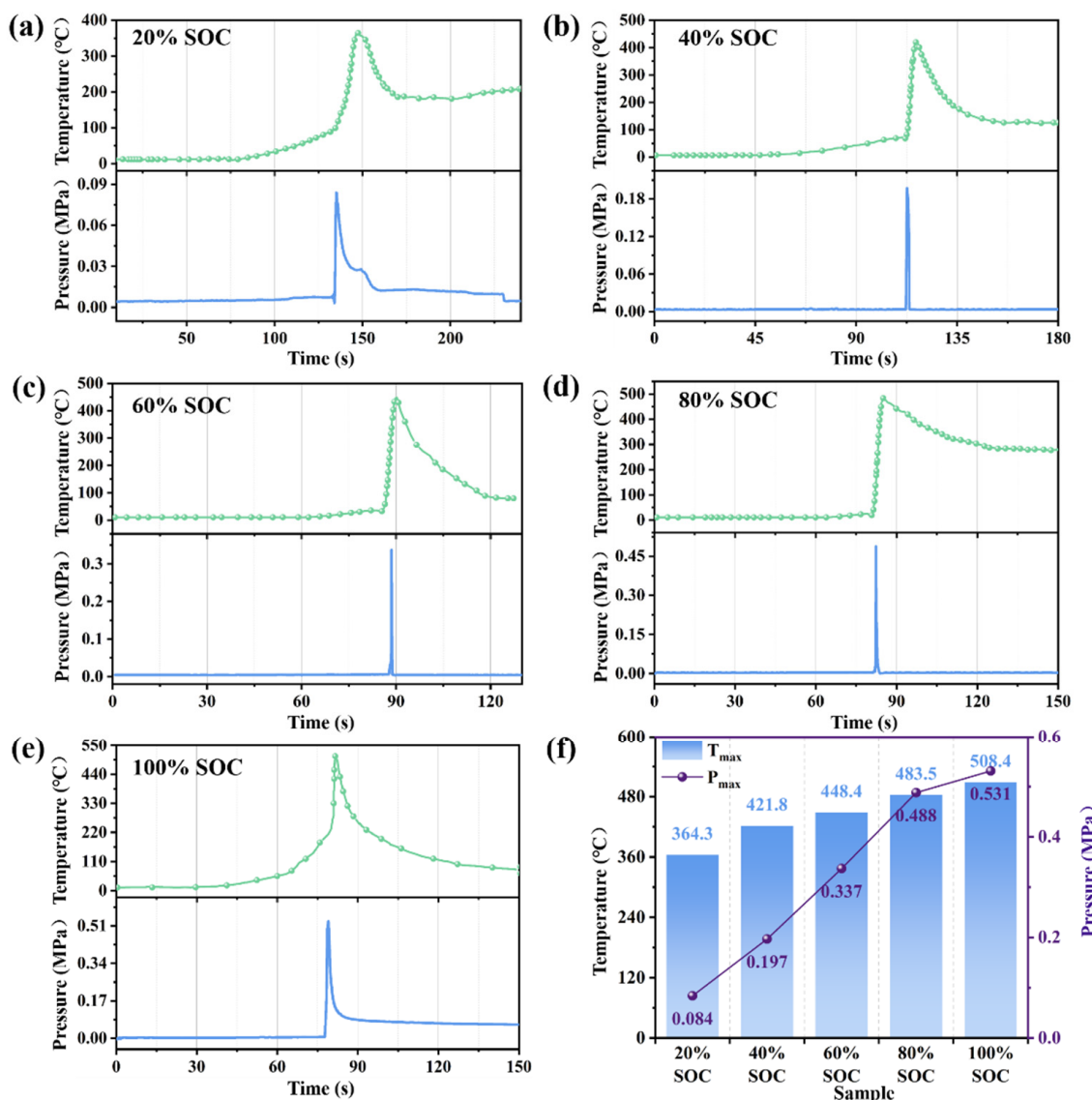


Figure 3. Variation in temperature and pressure with reaction time at the cathode direction during thermal runaway of lithium-ion batteries under different SOC conditions: 20% SOC (a), 40% SOC (b), 60% SOC (c), 80% SOC (d), 100% SOC (e); peak values of temperature and pressure under different SOC conditions (f).

Under different SOC conditions, the peak pressure and peak temperature of lithium-ion battery thermal runaway showed a similar trend. With the increase in SOC, the peak pressure also increased. When it reached 100% SOC, the peak pressure reached 0.531 MPa. At the same time, with the increase in SOC, the time to reach the peak pressure also moves

forward. However, different from the temperature, the change in battery pressure under any SOC state is instantaneous, and the battery pressure reaches the peak in an extremely short time and drops rapidly. In addition, due to the increase in internal pressure due to gas generation during the thermal runaway process of the lithium-ion battery, when the internal pressure reaches the limit, the gas affected by the pressure relief valve will instantly spray out along the positive direction of the battery and damage the positive structure of the battery. At the same time, because the large amount of gas generated is combustible gas, a jet flame will be generated along the positive direction of the battery to further improve the positive temperature. After the fire spraying phenomenon is over, an obvious explosion occurs inside the cell, accelerating the temperature rise and reaching the temperature peak. Therefore, under any SOC condition, the pressure peak appears earlier than the temperature peak.

3.3. Establishment and Simulation Analysis of Multi-Physics Coupling Model

3.3.1. Establishment of Multi-Physics Coupling Model

In order to solve the related problems of thermal runaway protection of lithium-ion battery packs, it is necessary to study the thermal runaway characteristics of lithium-ion battery packs. Firstly, based on the experimental results of thermal runaway of a single lithium-ion battery under 100% SOC as a reference, a multi-field coupling model of temperature pressure hydrodynamics under the condition of lithium-ion battery overheating runaway was established, and then the simulation model of thermal runaway characteristics of a single lithium-ion battery was repeated and the parameters were adjusted. Finally, the simulation study of lithium-ion battery overheating runaway characteristics was completed.

Under the condition of 100% SOC, the temperature and pressure changes in the positive direction of a single lithium-ion battery under thermal runaway are shown in Figure 3e, the temperature and pressure changes in the middle and bottom of the battery are shown in Figure S1, and the gas production during thermal runaway is shown in Table S1.

Based on the chemical reaction dynamics of lithium-ion battery thermal runaway and the interaction of multiple physical fields, the multi-field coupling control equation of temperature pressure hydrodynamics was constructed. Considering the coupling effect of heat conduction, chemical reaction heat release, and Joule heat, the temperature field equation can be established as:

$$\rho C_p \frac{\partial T}{\partial t} = \nabla \cdot (k \nabla T) + Q_{chem} + Q_{joule} \quad (1)$$

$$Q_{chem} = \sum_i \Delta H_i \cdot A_i \cdot e^{-E_{a,i}/(RT)} \cdot C_i^n \quad (2)$$

$$Q_{joule} = \sigma |\nabla \phi|^2 \quad (3)$$

where Q_{chem} is the heat from exothermic auxiliary reactions, ΔH_i is the enthalpy change of the reaction, C_i is the concentration of reactants, Q_{joule} is the Joule heat generated by internal short circuits, σ is the electrical conductivity, and ϕ is the electric potential field. For specific supplementary explanations on the temperature field equation and parameter values, please refer to the Supporting Information and Table S2.

Based on the gas state equation and the law of mass conservation, the pressure field equation can be established as:

$$\frac{\partial(\rho_g)}{\partial t} + \nabla \cdot (\rho_g u) = \sum_j S_{gas,j} \quad (4)$$

$$\rho_g \left(\frac{\partial u}{\partial t} + u \cdot \nabla u \right) = -\nabla p + \mu \nabla^2 u + F_{thermal} \quad (5)$$

$$F_{thermal} = \rho_g \beta (T - T_0) g \quad (6)$$

where $S_{gas,j}$ represents the j -th gas source, $F_{thermal}$ denotes thermal buoyancy, and β is the thermal expansion coefficient.

For the multi-component gas in the process of thermal runaway gas production of lithium-ion batteries, the gas component transport equation can be established as:

$$\frac{\partial C_j}{\partial t} + \nabla \cdot (C_j u) = \nabla \cdot (D_j \nabla C_j) + R_j \quad (7)$$

$$R_j = k_j e^{-E_{a,j}/(RT)} \prod C_i^m \quad (8)$$

where R_j is the generation rate of the j -th gas.

3.3.2. Construction of a Single Lithium-Ion Battery Thermal Runaway Simulation Model

In order to verify the accuracy of the temperature pressure hydrodynamics multi-field coupling control equation for the thermal runaway characteristics of lithium-ion batteries, Figure 4 shows the temperature distribution and pressure distribution at different times under the condition of thermal runaway of a single lithium-ion battery. According to the experimental conditions, the temperature measuring points in the model are arranged on the positive, middle, and negative surfaces of the battery. The pressure measuring points are arranged at 15 cm above the positive center of the battery, 10 cm on the side of the central axis of the battery, and 15 cm below the negative center of the battery. It can be seen from Figure 4a that with the process of thermal runaway of the battery, the cell temperature continues to rise. From the surface temperature distribution of the cell, the positive temperature of the cell is higher than the middle temperature of the cell, the middle temperature of the cell is higher than the negative temperature of the cell, and the maximum positive temperature of the battery reaches 500 °C. When the temperature increase in the battery surface reaches 50 °C, the internal pressure of the cell begins to produce gas; obviously, the internal pressure will destroy the pressure relief port, and a large amount of gas will be ejected from the pressure relief port on the positive side, forming jet fire. The maximum flame temperature near the pressure relief port is about 973 k, and the flame temperature at a distance of 2 cm above the pressure relief port is about 700 k, and the fire spraying process lasts about 10 s. There is a large air velocity of 17.9 m/s near the pressure relief port. In the air domain, the overall air velocity in the area above the positive electrode is in the range of 3.6–7.2 m/s (Figure 4b). After the end of the fire spraying phenomenon, a relatively obvious explosion occurred inside the cell. At this time, the positive end face was damaged, the material inside the cell was ejected from the positive end face, and an obvious pressure wave was captured at the pressure monitoring point. The overpressure near the positive electrode of the battery can reach more than 0.5 MPa. When the pressure wave propagates to the top of the container, it is reflected off the wall. The peak overpressure captured by the pressure monitoring point on the top wall can reach 0.4 MPa (Figure 4c). It can be seen that the thermal runaway simulation model of a single lithium-ion battery based on the temperature pressure hydrodynamics multi-field coupling control equation is in good agreement with the experimental data, and the control equation can be used to further study the thermal runaway characteristics of lithium-ion batteries.

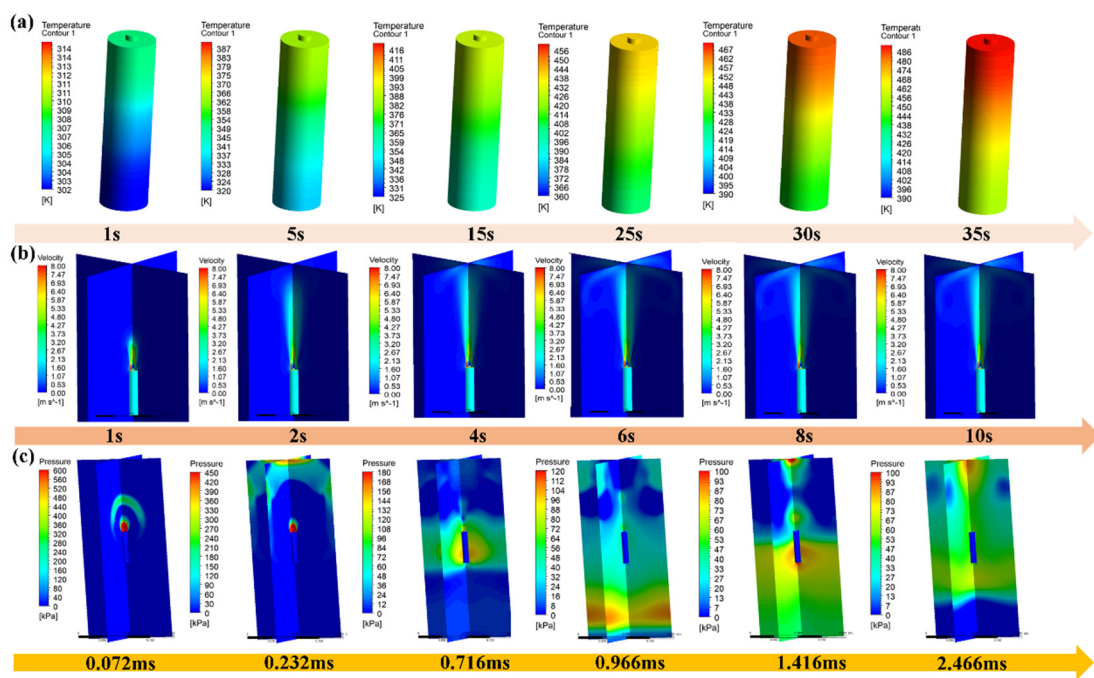


Figure 4. Temperature distribution at different time instants under thermal runaway conditions of a single lithium-ion battery (a), airflow velocity distribution in the air (b), and pressure distribution (c).

3.3.3. Construction of Thermal Runaway Simulation Model for Lithium-Ion Battery Pack

According to the thermal runaway characteristics of lithium-ion battery pack, a $4 \times 4 \times 4$ combined arrangement of battery pack is established by using the existing temperature pressure hydrodynamics multi-field coupling control equation. The thermal runaway occurs in eight cells ($2 \times 2 \times 2$) inside the battery pack. The thermal runaway simulation results are shown in Figures 5 and 6. The temperature distribution at different times under the condition of thermal runaway of the lithium-ion battery pack is shown in Figure 5. It can be seen that after the jet fire stage, the bottom temperature of the upper cell can reach 1047°C , and the side temperature can reach 500°C . Because the temperature has been far higher than the thermal stability temperature of lithium-ion batteries, the risk of thermal runaway on both sides of the cells is high, and the risk of thermal runaway of the batteries on both sides is higher due to the layout of the battery pack. After the end of the jet fire phase, the runaway cell explodes, and the pressure change in the air region where the lithium-ion battery pack is located during the explosion is shown in Figure 6. It can be seen from the figure that during the explosion of the battery module, the phenomenon of pressure convergence and reflection is more complex than that of a single cell. After the explosion, the pressure wave first propagates from the positive pole of the thermal runaway cell to the upper space. After being blocked by the upper cell, it generates a downward propagating reflected wave. During the explosion, the maximum overpressure on the surface of the upper cell can reach 0.8 MPa. For the thermal runaway of the lithium-ion battery pack in the confined space, the explosion pressure in the negative direction of the battery pack is relatively small, and the shock wave is mainly concentrated in the middle and upper part of the lithium-ion battery pack, which also provides a favorable reference for the risk prevention and control of the lithium-ion battery pack, sensor layout and core thread layout. However, in practical applications, due to the influence of the structural strength and spatial state of the external protective layer of the lithium-ion battery pack, its damage to the external environment is greatly different. Therefore, when setting pressure relief valves, sensors, and external space redundancy, the out-of-control model of the lithium-ion

battery under the condition of multi-physical field coupling should be further regulated according to the actual situation.

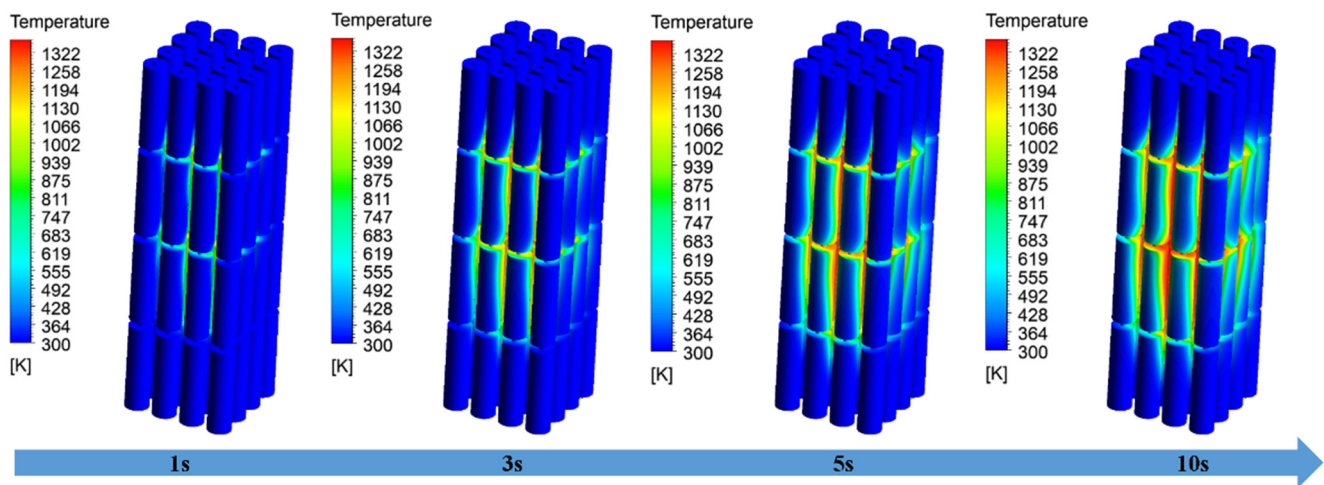


Figure 5. Temperature distribution of lithium-ion battery pack under thermal runaway conditions at various time points.

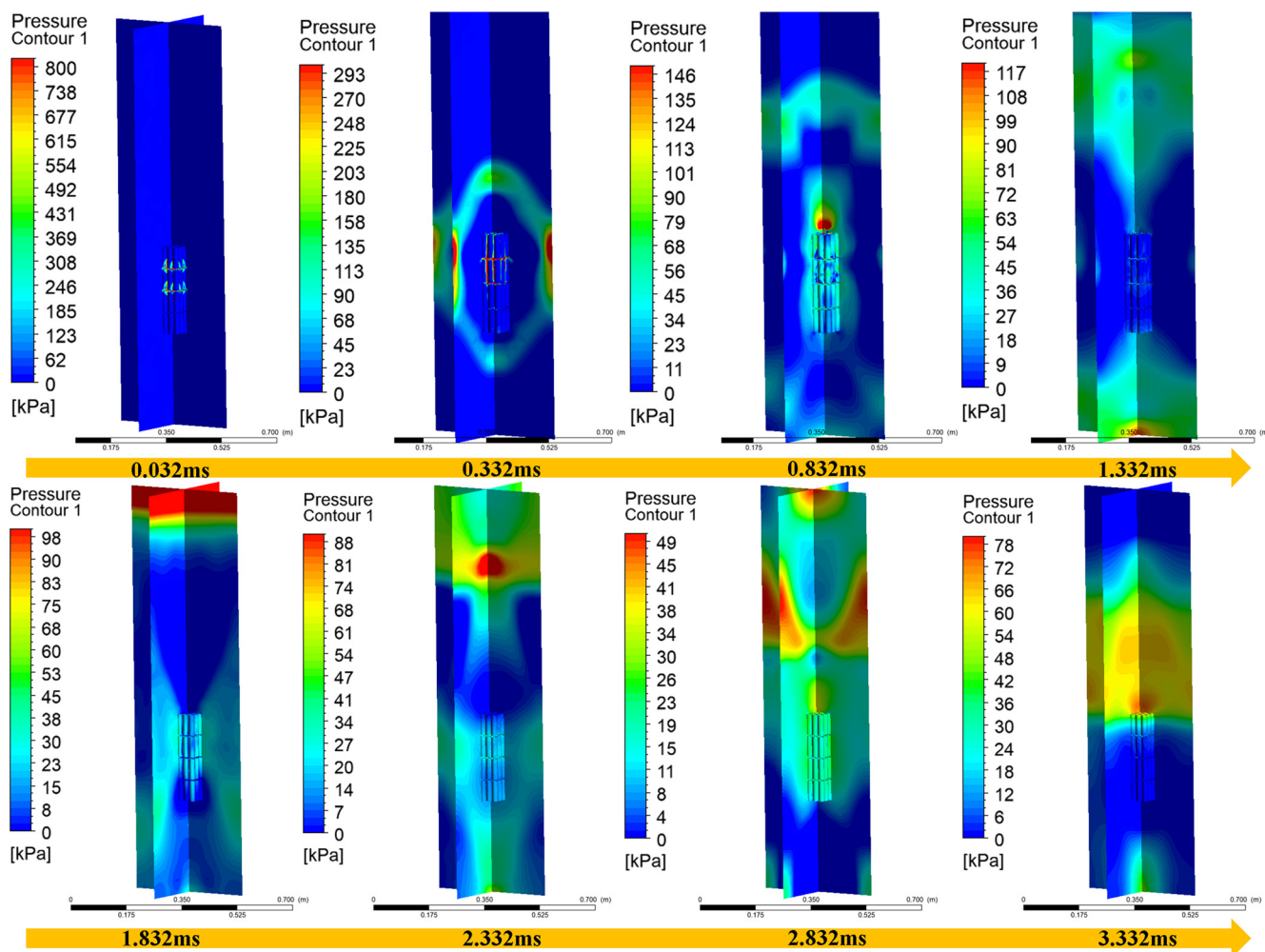


Figure 6. The pressure distribution of the lithium-ion battery pack under thermal runaway conditions at different time points.

4. Conclusions

This study systematically revealed the influence of different states of charge (SOC) on the thermal runaway behavior of lithium-ion batteries and its internal mechanism. The experimental results show that SOC can significantly change the thermal runaway characteristics by regulating the internal oxidation–reduction balance of the battery: under the condition of high SOC, the lithium-rich positive electrode accelerates the release of lattice oxygen, causes violent oxidation reaction, and the thermal runaway intensity is significantly enhanced; under the condition of low SOC, the reduction environment is dominant and the peak temperature is low, but the risk of lithium precipitation may aggravate the internal short circuit. The multi-physical field coupling model accurately reproduced the thermal runaway evolution process of monomer and module level through the dynamic correlation of temperature pressure hydrodynamics. The simulation results show that it is necessary to optimize the thermal management strategy of battery pack based on SOC, limit the operation threshold of high SOC battery, and block the thermal pressure coupling propagation path through the directional design of pressure relief structure and the optimization of sensor layout, so as to improve the system level security. To sum up, the research results laid a theoretical and technical foundation for the development of lithium-ion battery precise safety protection and high-performance energy storage systems.

Supplementary Materials: The following supporting information can be downloaded at: <https://www.mdpi.com/article/10.3390/batteries11050202/s1>, Table S1. The composition of gas generated after thermal runaway of the lithium-ion battery; Table S2. Parameter Values of the Internal heat generation model of lithium-ion batteries [39]. Figure S1. The temperature and pressure changes in the middle and bottom of the battery.

Author Contributions: Conceptualization, Y.Y.; formal analysis, Y.Y., X.P. and L.G.; investigation, Y.Y. and Z.Z.; methodology, Z.Z., H.X. and X.X.; resources, Y.Q. and S.Y.; software, X.P.; validation, J.G., L.L. and Y.W.; writing—review and editing, Z.Z. All authors will be updated at each stage of manuscript processing, including submission, revision, and revision reminder, via emails from our system or the assigned Assistant Editor. All authors have read and agreed to the published version of the manuscript.

Funding: This work was supported by the State Key Laboratory of Disaster Prevention & Mitigation of Explosion & Impact (No. LGD-SKL-202203), the Nature Science Foundation of Jiangsu Province (No. BK20241602), and the Army Engineering University Youth Independent Innovation Fund (No.KYFYJKQTZQ23006).

Data Availability Statement: The data that support the findings of this study are available from the corresponding author upon reasonable request.

Conflicts of Interest: The authors declare no conflicts of interest.

References

1. Kim, T.; Song, W.T.; Son, D.Y.; Ono, L.K.; Qi, Y.B. Lithium-ion batteries: Outlook on present, future, and hybridized technologies. *J. Mater. Chem. A* **2019**, *7*, 2942–2964. [[CrossRef](#)]
2. Li, M.; Lu, J.; Chen, Z.W.; Amine, K. 30 Years of Lithium-Ion Batteries. *Adv. Mater.* **2018**, *30*, 1800561. [[CrossRef](#)] [[PubMed](#)]
3. Manthiram, A. An Outlook on Lithium Ion Battery Technology. *ACS Cent. Sci.* **2017**, *3*, 1063–1069. [[CrossRef](#)]
4. Zubi, G.; Dufo-Lopez, R.; Carvalho, M.; Pasaoglu, G. The lithium-ion battery: State of the art and future perspectives. *Renew. Sustain. Energy Rev.* **2018**, *89*, 292–308. [[CrossRef](#)]
5. Zeng, X.; Li, M.; Abd El-Hady, D.; Alshitari, W.; Al-Bogami, A.S.; Lu, J.; Amine, K. Commercialization of Lithium Battery Technologies for Electric Vehicles. *Adv. Energy Mater.* **2019**, *9*, 1900161. [[CrossRef](#)]
6. Cheng, X.-B.; Liu, H.; Yuan, H.; Peng, H.-J.; Tang, C.; Huang, J.-Q.; Zhang, Q. A perspective on sustainable energy materials for lithium batteries. *Susmat* **2021**, *1*, 38–50. [[CrossRef](#)]

7. Uitz, M.; Sternad, M.; Breuer, S.; Täubert, C.; Traussnig, T.; Hennige, V.; Hanzu, I.; Wilkening, M. Aging of Tesla's 18650 Lithium-Ion Cells: Correlating Solid-Electrolyte-Interphase Evolution with Fading in Capacity and Power. *J. Electrochem. Soc.* **2017**, *164*, A3503–A3510. [[CrossRef](#)]
8. Hollinger, A.S.; McAnallen, D.R.; Brockett, M.T.; DeLaney, S.C.; Ma, J.; Rahn, C.D. Cylindrical lithium-ion structural batteries for drones. *Int. J. Energy Res.* **2020**, *44*, 560–566. [[CrossRef](#)]
9. Duh, Y.S.; Sun, Y.J.; Lin, X.; Zheng, J.J.; Wang, M.C.; Wang, Y.J.; Lin, X.Y.; Jiang, X.Y.; Zheng, Z.G.; Zheng, S.; et al. Characterization on thermal runaway of commercial 18650 lithium-ion batteries used in electric vehicles: A review. *J. Energy Storage* **2021**, *41*, 102888. [[CrossRef](#)]
10. Lee, P.-Y.; Kim, J.; Choi, Y.-O.; Kim, C.-J. Comparative Analysis of 18650 Lithium-Ion Cylindrical Cells for Electric Vehicle (EV) and Battery Energy Storage System (BESS). *J. Adv. Eng. Technol.* **2017**, *10*, 131–137.
11. Panchal, S.; Mathew, M.; Fraser, R.; Fowler, M. Electrochemical thermal modeling and experimental measurements of 18650 cylindrical lithium-ion battery during discharge cycle for an EV. *Appl. Therm. Eng.* **2018**, *135*, 123–132. [[CrossRef](#)]
12. Feng, X.N.; Ouyang, M.G.; Liu, X.; Lu, L.G.; Xia, Y.; He, X.M. Thermal runaway mechanism of lithium ion battery for electric vehicles: A review. *Energy Storage Mater.* **2018**, *10*, 246–267. [[CrossRef](#)]
13. Mallick, S.; Gayen, D. Thermal behaviour and thermal runaway propagation in lithium-ion battery systems-A critical review. *J. Energy Storage* **2023**, *62*, 106894. [[CrossRef](#)]
14. Hu, X.J.; Gao, F.F.; Xiao, Y.; Wang, D.P.; Gao, Z.H.; Huang, Z.F.; Ren, S.D.; Jiang, N.; Wu, S.T. Advancements in the safety of Lithium-Ion Battery: The Trigger, consequence and mitigation method of thermal runaway. *Chem. Eng. J.* **2024**, *481*, 148450. [[CrossRef](#)]
15. Zhang, X.; Li, Z.; Luo, L.; Fan, Y.; Du, Z. A review on thermal management of lithium-ion batteries for electric vehicles. *Energy* **2022**, *238*, 121652. [[CrossRef](#)]
16. Xu, L.; Wang, S.; Li, Y.; Li, Y.; Sun, J.; Zhao, F.; Wang, H.; Wang, Y.; Xu, C.; Feng, X. Thermal runaway propagation behavior and gas production characteristics of NCM622 battery modules at different state of charge. *Process Saf. Environ. Prot.* **2024**, *185*, 267–276. [[CrossRef](#)]
17. Liu, Y.; Zhang, L.; Ding, Y.; Huang, X.; Huang, X. Effect of thermal impact on the onset and propagation of thermal runaway over cylindrical Li-ion batteries. *Renew. Energy* **2024**, *222*, 119910. [[CrossRef](#)]
18. Yang, Y.; Wang, R.J.; Shen, Z.J.; Yu, Q.Q.; Xiong, R.; Shen, W.X. Towards a safer lithium-ion batteries: A critical review on cause, characteristics, warning and disposal strategy for thermal runaway. *Adv. Appl. Energy* **2023**, *11*, 100146. [[CrossRef](#)]
19. Wang, K.; Wu, D.J.; Chang, C.Y.; Zhang, J.Q.; Ouyang, D.X.; Qian, X.M. Charging rate effect on overcharge-induced thermal runaway characteristics and gas venting behaviors for commercial lithium iron phosphate batteries. *J. Clean. Prod.* **2024**, *434*, 139992. [[CrossRef](#)]
20. Qi, C.; Liu, Z.Y.; Lin, C.J.; Liu, X.; Liu, D.H.; Li, Z.Y.; Yi, A.B. The gas production characteristics and catastrophic hazards evaluation of thermal runaway for $\text{LiNi}_{0.5}\text{Co}_{0.2}\text{Mn}_{0.3}\text{O}_2$ lithium-ion batteries under different SOCs. *J. Energy Storage* **2024**, *88*, 111678. [[CrossRef](#)]
21. Chuang, Q.; Hongtao, Y.; Ju, Y.; Chunjing, L.; Yapeng, Z.; Yuanzhi, H.; Bin, C. Study on the characteristics of thermal runaway expansion force of $\text{LiNi}_{0.5}\text{Co}_{0.2}\text{Mn}_{0.3}\text{O}_2$ /graphite lithium-ion batteries with different SOCs. *Electrochim. Acta* **2024**, *495*, 144448. [[CrossRef](#)]
22. Zhou, G.; Yang, S.; Liu, Y.; Wang, J.; Bian, Y.; Yu, H.; Zhang, Q.; Li, Y.; Niu, C. Experimental study on thermal runaway propagation characteristics of NCM811 lithium-ion batteries with different SOCs induced by dual heat sources. *Int. Commun. Heat Mass Transf.* **2023**, *149*, 107089. [[CrossRef](#)]
23. Hong, J.C.; Wang, Z.P.; Qu, C.H.; Zhou, Y.J.; Shan, T.X.; Zhang, J.H.; Hou, Y.K. Investigation on overcharge-caused thermal runaway of lithium-ion batteries in real-world electric vehicles. *Appl. Energy* **2022**, *321*, 119229. [[CrossRef](#)]
24. Kong, D.P.; Zhao, H.L.; Ping, P.; Zhang, Y.; Wang, G.Q. Effect of low temperature on thermal runaway and fire behaviors of 18650 lithium-ion battery: A comprehensive experimental study. *Process Saf. Environ. Prot.* **2023**, *174*, 448–459. [[CrossRef](#)]
25. Ren, D.S.; Feng, X.N.; Liu, L.S.; Hsu, H.J.; Lu, L.G.; Wang, L.; He, X.M.; Ouyang, M.G. Investigating the relationship between internal short circuit and thermal runaway of lithium-ion batteries under thermal abuse condition. *Energy Storage Mater.* **2021**, *34*, 563–573. [[CrossRef](#)]
26. Wang, H.B.; Xu, H.; Zhang, Z.L.; Wang, Q.Z.; Jin, C.Y.; Wu, C.J.; Xu, C.S.; Hao, J.Y.; Sun, L.; Du, Z.M.; et al. Fire and explosion characteristics of vent gas from lithium-ion batteries after thermal runaway: A comparative study. *Etransportation* **2022**, *13*, 100190. [[CrossRef](#)]
27. Alkhedher, M.; Al Tahhan, A.B.; Yousaf, J.; Ghazal, M.; Shahbazian-Yassar, R.; Ramadan, M. Electrochemical and thermal modeling of lithium-ion batteries: A review of coupled approaches for improved thermal performance and safety lithium-ion batteries. *J. Energy Storage* **2024**, *86*, 111172. [[CrossRef](#)]
28. Wu, H.; Chen, S.; Hong, Y.; Xu, C.; Zheng, Y.; Jin, C.; Chen, K.; He, Y.; Feng, X.; Wei, X.; et al. Thermal safety boundary of lithium-ion battery at different state of charge. *J. Energy Chem.* **2024**, *91*, 59–72. [[CrossRef](#)]

29. Wang, Q.S.; Ping, P.; Zhao, X.J.; Chu, G.Q.; Sun, J.H.; Chen, C.H. Thermal runaway caused fire and explosion of lithium ion battery. *J. Power Sources* **2012**, *208*, 210–224. [[CrossRef](#)]
30. Li, Y.; Liu, X.; Wang, L.; Feng, X.N.; Ren, D.S.; Wu, Y.; Xu, G.L.; Lu, L.G.; Hou, J.X.; Zhang, W.F.; et al. Thermal runaway mechanism of lithium-ion battery with $\text{LiNi}_{0.8}\text{Mn}_{0.1}\text{Co}_{0.1}\text{O}_2$ cathode materials. *Nano Energy* **2021**, *85*, 105878. [[CrossRef](#)]
31. Zhang, G.X.; Wei, X.Z.; Zhu, J.G.; Chen, S.Q.; Han, G.S.; Dai, H.F. Revealing the failure mechanisms of lithium-ion batteries during dynamic overcharge. *J. Power Sources* **2022**, *543*, 231867. [[CrossRef](#)]
32. Liu, X.; Ren, D.S.; Hsu, H.J.; Feng, X.N.; Xu, G.L.; Zhuang, M.H.; Gao, H.; Lu, L.G.; Han, X.B.; Chu, Z.Y.; et al. Thermal Runaway of Lithium-Ion Batteries without Internal Short Circuit. *Joule* **2018**, *2*, 2047–2064. [[CrossRef](#)]
33. Finegan, D.P.; Scheel, M.; Robinson, J.B.; Tjaden, B.; Hunt, I.; Mason, T.J.; Millichamp, J.; Di Michiel, M.; Offer, G.J.; Hinds, G.; et al. In-operando high-speed tomography of lithium-ion batteries during thermal runaway. *Nat. Commun.* **2015**, *6*, 6924. [[CrossRef](#)] [[PubMed](#)]
34. Liao, Z.H.; Zhang, S.; Li, K.; Zhao, M.Y.; Qiu, Z.J.; Han, D.; Zhang, G.Q.; Habetsler, T.G. Hazard analysis of thermally abused lithium-ion batteries at different state of charges. *J. Energy Storage* **2020**, *27*, 101065. [[CrossRef](#)]
35. Zhang, Q.S.; Niu, J.H.; Zhao, Z.H.; Wang, Q. Research on the effect of thermal runaway gas components and explosion limits of lithium-ion batteries under different charge states. *J. Energy Storage* **2022**, *45*, 103759. [[CrossRef](#)]
36. Mao, B.B.; Huang, P.F.; Chen, H.D.; Wang, Q.S.; Sun, J.H. Self-heating reaction and thermal runaway criticality of the lithium ion battery. *Int. J. Heat Mass Transf.* **2020**, *149*, 119178. [[CrossRef](#)]
37. Lyu, P.Z.; Liu, X.J.; Qu, J.; Zhao, J.T.; Huo, Y.T.; Qu, Z.G.; Rao, Z.H. Recent advances of thermal safety of lithium ion battery for energy storage. *Energy Storage Mater.* **2020**, *31*, 195–220. [[CrossRef](#)]
38. Yang, M.; Rong, M.; Ye, Y.; Yang, A.; Chu, J.; Yuan, H.; Wang, X. Comprehensive analysis of gas production for commercial LiFePO_4 batteries during overcharge-thermal runaway. *J. Energy Storage* **2023**, *72*, 108323. [[CrossRef](#)]
39. Zhang, Q.; Jia, Y.; Zhai, Q.; Liu, T. Simulation Research on Thermal Runaway Heat Transfer of Lithium-ion Batteries in Confined Space. *J. Saf. Sci.* **2024**, *34*, 65.

Disclaimer/Publisher’s Note: The statements, opinions and data contained in all publications are solely those of the individual author(s) and contributor(s) and not of MDPI and/or the editor(s). MDPI and/or the editor(s) disclaim responsibility for any injury to people or property resulting from any ideas, methods, instructions or products referred to in the content.